

METHODS

Porous Polypropylene Membrane Based pH Sensing for Skin Monitoring

KHENGDAULIU CHAWANG¹, SHIH-CHENG CHOU²,
SEN BING¹, (Graduate Student Member, IEEE), PU-WEI WU²,
AND J.-C. CHIAO¹, (Fellow, IEEE)

¹Department of Electrical and Computer Engineering, Southern Methodist University, Dallas, TX 75205, USA

²Department of Materials Science and Engineering, National Yang Ming Chiao Tung University, Hsinchu 300, Taiwan

Corresponding author: Khengdauliu Chawang (kchawang@smu.edu)

This work was supported in part by the School of Engineering, Southern Method University, Mary and Richard Templeton Endowment, the Ministry of Science and Technology of Taiwan, under Grant 110-2221-E-A49-060; in part by the Higher Education Sprout Project by the Ministry of Education (MOE) in Taiwan for Center for Neuromodulation Medical Electronics Systems; and in part by the Higher Education Sprout Project of the National Yang Ming Chiao Tung University and MOE, Taiwan.

ABSTRACT An iridium oxide-based electrical pH sensor that is suitable to be embedded in an electronic bandage for skin monitoring has been developed. The electrical pH sensor does not entail high-temperature fabrication processes thus is suitable to be built on polypropylene micro membrane (PPMM), a paper-like substrate, which is inert, gas-permeable, and biomechanically-compatible to tissue. The PPMM was metalized by an electroless gold-coating process and iridium oxide nanoparticles were electrodeposited on the porous membranes. The reference electrode was made by screen printing Ag/AgCl paste on the substrate. pH responses of the IrO₂ PPMM against a commercial reference electrode or the planar Ag/AgCl reference electrode were examined. A super-Nernstian sensitivity of -66.8 mV/pH was achieved with the PPMM-based sensor in a pH range from pH 2 to 13. The electrodes also produced similar responses in smaller pH ranges of pH 5 to 8 and around pH 7. Output potential characterization, such as cyclic voltammetry, hysteresis, response time, potential drift, deviation, fluctuation, and potential stability, showed repeatable and stable pH responses in physiologically relevant pH ranges. Interference factors such as salt concentration, viscosity and temperature have also been investigated. The results show that the calibration procedures should consider these factors specific to targeted applications. The planar pH-sensitive electrodes show reliable performance in a bandage configuration designed and packaged for wound monitoring. The accuracy assessment in a Clarke error grid and the result of sensing pH induced by uric acid showed the feasibility of bandage applications. The electrical and biocompatible electrodes embedded in breathable porous bandages can be integrated with portable electronics to be used as wearables for wireless tissue monitoring.


INDEX TERMS pH sensor, planar, iridium oxide, polypropylene micro membrane, electronic bandage.

I. INTRODUCTION

The pH response of iridium oxide (IrO₂) has been studied to be advantageous over other metal oxides [1], [2] owing to a higher sensitivity over a wide pH range and on different substrates [3], even at varying temperatures [4] and in non-aqueous environment [5]. It is also a widely used bioelectrode material for implantable devices due to its high charge

density [6], [7], [8], [9], biocompatibility and low impedance [10], [11], [12], [13]. The electro-conductive property of IrO₂ film makes it a promising material choice for electrical sensing in integrated wearable and implantable devices [14].

Early studies of IrO₂ pH responses were commonly performed on rigid substrates like glassy carbon [15], [16] and iridium wires [17], [18], [19], [20], [21] which are not suitable for wearable applications. Advancements in material research have allowed the deposition of IrO₂ film on flexible substrates, such as by sputtering [22], [23], [24],

The associate editor coordinating the review of this manuscript and approving it for publication was Derek Abbott .

sol-gel [25], [26], [27], and multi-step electrodeposition [28], [29]. Flexible substrates enable the sensor use in wearables. The sputtering process requires deliberate plasma coverage uniformity for the conformal coating in order to produce high pH performance. Sol-gel processes to prepare iridium oxide involve a high temperature above 325 °C for oxide formation [30]. These fabrication methods require a flexible substrate to be able to withstand not only a high temperature for a period of time, but also thermal expansion coefficient mismatch between the substrate, metal, and oxide, which results in film wrinkles and delamination.

Electrodeposition at room temperature seems to be a promising process for conformal and uniform coating on flexible substrates [31], [32], [33], particularly, in which paper-based substrates are used for microfluidic and low-cost analytical point-of-care devices. The electrodeposition technique has been reported to produce super Nernstian or Nernstian sensitivities on rigid glass [15], [34]. Recently, flexible polyimide [35], [36] and soft porous polymeric substrates have also been utilized to produce similar pH sensitivities [37].

In this study, a flexible IrO₂ pH sensor based on porous substrates suitable for skin monitoring was proposed. The substrate, similar to the ones used in paper-based microfluidic devices [38], [39] is commercially-available polypropylene (PP), one of the widely used polymers. To distinguish the common use of polypropylene (PP) films that can be any thickness or pore size, the thin film used in our fabrication is called polypropylene micro membrane (PPMM). The porometer analysis showed the PPMM has an average flow pore diameter of 0.247 μm and a pore flow pressure of 17.562 psi [40]. The porous gas-permeable PPMM is also known to be inert, foul resistant and biocompatible with robust mechanical strength and chemical resistance [41], [42], [43], [44].

Our group has previously demonstrated the performance of the sensing film with the IrO₂ nanoparticles coated on the metalized PPMM [37], [40], [45], [46] against a bulky commercial reference electrode. In this work, the pH-sensitive film electrode is further integrated with a planar Ag/AgCl film as the reference electrode. The fabrication of the sensing film is briefly described here. The PPMM was gold (Au) metalized by an electroless process [40], [45], and IrO₂ nanoparticles were further deposited by an electrochemical process using IrO₂ colloid suspension [47]. Electroless metallization of gold on individual PPMM fibers used polydopamine (PDA) and poly vinyl alcohol (PVA) as the adhesive, wetting, and reducing agents to improve their hydrophilicity of PPMM fibers. The metalized fiber had a gold thickness of 150 nm, transversely encapsulating individual PPMM fibers. The measured conductivity was 0.1 S/cm. A conductive polymer membrane allowed electrical interfacing between the sensing film and electronics on paper-based devices. In addition, the metallization process of PPMM fibers was needed to electroplate the IrO₂ layer. The electrodeposition of IrO₂ nanoparticles on metalized

PPMM (named as PPMM@Au) did not entail vacuum or high temperatures.

The planar IrO₂ coated on PPMM@Au was named PWE to be used as the working electrode. A planar reference electrode was prepared by screen printing Ag/AgCl paste and named as KRE. The PWE against KRE was tested in the skin wound pH range which changes from alkaline to acidic during the healing process [48]. Typically, pH sensitivities were obtained without interfering effects of salt. Body fluid contains sodium and potassium [49]. The addition of salt in an aqueous pH solution created a pH difference which has previously been demonstrated by using planar nonporous IrO_x electrodes [50]. In this work, the planar porous PWE and KRE electrodes were tested in sodium and potassium salt-added solutions. Similarly, Yang et al. have demonstrated and suggested that integrating a NaCl sensor could correct the output potentials in aqueous pH solutions for nonporous pH sensors [51].

Calibration in aqueous solutions may produce pH variations in viscous solutions due to the effects by the changed ionic mobility. Previously, Chawang et al. demonstrated pH change in viscous pH solutions [50]. Serous fluid released during the natural healing process of inflammation is viscous, which may alter the pH reading calculated by calibration using aqueous solutions. Thus, the porous IrO₂-coated PPMM@Au and planar Ag/AgCl electrodes were tested in viscous environments. To demonstrate the use of conductive and porous PPMM bioelectrode in skin wound monitoring, planar electrodes were assembled in an electronic bandage. Conductive lines were screen printed on a bandage and a porous absorbing layer was used for liquid transfusion. The pH accuracy was analyzed in a Clarke error grid.

II. MATERIALS AND METHODS

A. ELECTRODE FABRICATION

Polyvinyl (PVA) and polydopamine (PDA) (Merck, Darmstadt, Germany) were conformally deposited on individual polypropylene (PP) fibers to improve their hydrophilicity. The polypropylene micro membrane (PPMM) (Rone Scientific Inc., Kaohsiung, Taiwan) had a nominal pore size of 450 nm and a thickness of 200 μm. For the hydrophilic treatment, PPMM was immersed in 0.01 M Tris buffer at 25°C for 20 h, prepared by mixing 2 mg/mL of dopamine hydrochloride (DA-HCl) (Acros Organic, Geel, Belgium) and 12.8 mg/mL PVA in deionized water and anhydrous ethanol with the volume ratio of 7:3. Next, the hydrophilic PPMM was activated for metallization by immersing in 0.1 M hydrogen tetrachloroaurate (III) trihydrate (HAuCl₄) (Alfa Aesar, Massachusetts, USA) (pH 5.2) for 10 min. The activated PPMM was transferred for electroless Au plating in a bath solution containing 0.05 M HAuCl₄, 0.4 M citrate acid, 0.02 M Na₂SO₃, and 0.04 M Na₂S₂O₃ mixed in 20 mL deionized water (DI). Afterward, 0.792 mg sodium L-ascorbate was added to the aqueous bath solution to initiate Au⁺ reduction and the temperature was raised to 30°C for 2 h. Finally,

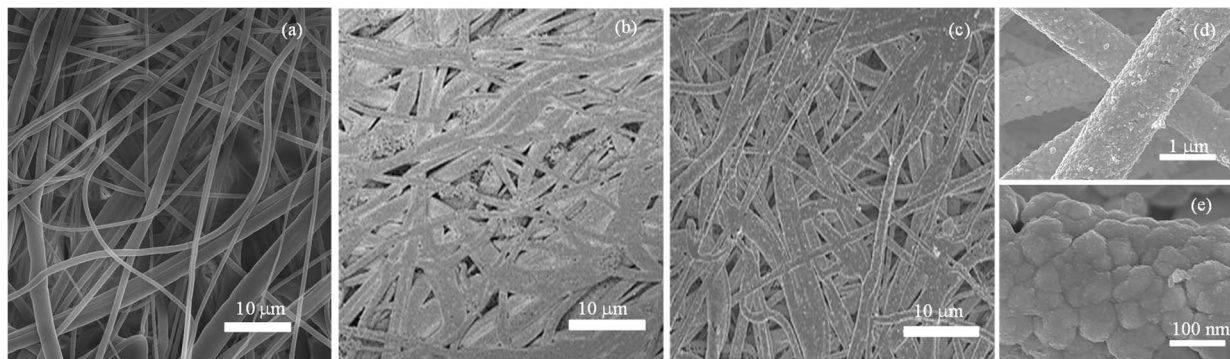


FIGURE 1. SEM images of (a) bare PPMM fibers, (b) metallized PPMM@Au fibers, and (c)-(e) PWE fibers in different magnifications.

the metallized PPMM (PPMM@Au) was washed in DI water. The pH values of the Tris buffer and Au plating solutions were 8.5 and 6.5, respectively. Previously, the mechanical strength and flexibility of PPMM@Au were demonstrated by bending the sample at 60°C for 10,000 bending cycles [40]. Thus, the connectivity for electrical signals should be secured after the mechanical bending of the film in wearables.

The IrO₂ nanoparticles were electrodeposited on the metallized film PPMM@Au for the pH sensing function using IrO₂ suspension reported [45]. The solution of 0.005-M potassium hexachloroiridate (K₂IrCl₆) was first adjusted to pH 12 by adding NaOH and then heated at 90°C for 20 min to form a colloidal suspension. Potentiostat (VersaSTAT4, AMETEK Inc., USA) was used for electrodeposition at 0.4 V for 30 min using a three-electrode cell system with Pt foil (2 × 2 cm²) as the counter electrode; PPMM@Au (1 × 1 cm²) as the working electrode; and a saturated calomel electrode (SCE) as the reference electrode. The finished sample was cut into 2 mm × 15 mm strips and named as PWE (polypropylene working electrode).

The Ag/AgCl reference electrode (named as KRE) was prepared by screen-printing Ag/AgCl paste (011464, ALS, Japan) on the substrate. A precision blade was used to ensure the smoothness of the thin paste layer on the substrate. It was dried for 10 minutes at room temperature and cut into individual 2 mm × 15 mm strips. Silver epoxy (8331D, MG Chemicals, USA) was used to connect copper wires on the PWE and KRE to a high-impedance buffer amplifier with a unity gain for electrical measurements.

B. MATERIALS

Commercial buffer solutions (Fisher Scientific, Hampton, NH, USA) were used for sensitivity studies at pH 2, 4, 5, 6, 7, 8, 10, and 13. A glass-bodied Ag/AgCl reference electrode (MF-2052, Basi, USA) with a flexible connector filled with a 3-M NaCl solution was used for comparison with our KRE.

Custom-made buffer solutions were prepared for sensitivity and sensor characterization experiments. Commercial buffer pH 8 (Fisher Scientific, Hampton, NH, USA) was used as the base solution and a digital benchtop pH meter

(A211, Thermo Scientific Orion, USA) was used to measure the pH values. Hydrochloric acid HCl (50%, LabChem, Zelenople, PA, USA) and sodium hydroxide NaOH (50%, Sigma-Aldrich, St. Louis, MO, USA) were used to decrease or increase the pH levels of the pH 8 buffer.

For viscosity variations, lab-grade starch powders (C₆H₁₀O₅)_n (Carolina Biological Supply Company, Burlington, NC, USA) were used as the thickening agent to prepare viscous solutions in order to investigate the effects of viscosity on output pH errors. Viscometer tubes of sizes 200 and 600 (CANNON Instrument Company, State College, PA, USA) were used. Viscous solutions by adding 1% and 2.4% starch by weight were prepared in different pH buffers. A commercial pH meter (A1311, Apera Instrument, USA) was used to compare pH values. Uric acid powder (UA2875-5G, Sigma Aldrich, USA) was used to prepare different Uric acid (UA) concentration solution. A data acquisition card (6201, National Instruments, USA) sampled at 7 S/s was used to record the potential difference between the working and reference electrodes.

III. RESULT AND DISCUSSION

A. CHARACTERIZATIONS

Scanning electron microscopy (SEM) was used to analyze the surface morphology. The bare PPMM fibers are shown in Fig. 1(a). The rough PPMM@Au fibers in Fig. 1(b) show successful deposition of Au nanoparticles. Figs. 1(c)-(e) show the denser fibers in PWE under different magnifications that IrO₂ nanoparticles were electrodeposited on the metallized PPMM@Au fibers.

Cyclic voltammetry (CV) experiments were performed over the physiologically relevant pH of 8 and 5. First, the CV measurements were conducted to compare the PWE against the planar Ag/AgCl KRE with a size of 2 mm × 15 mm, or the standard liquid-filled glass-bodied reference electrode (CRE) with a 6-mm diameter and 75-mm length (MF-2052, Basi, USA). An electrochemical analyzer (CHI7001D, CH Instruments, USA) was used for the CV experiment and phosphate buffer saline (PBS) solution was adjusted to pH 8 and pH 5, by adding 2-M NaOH and 2-M HCl, respectively into 50 mL

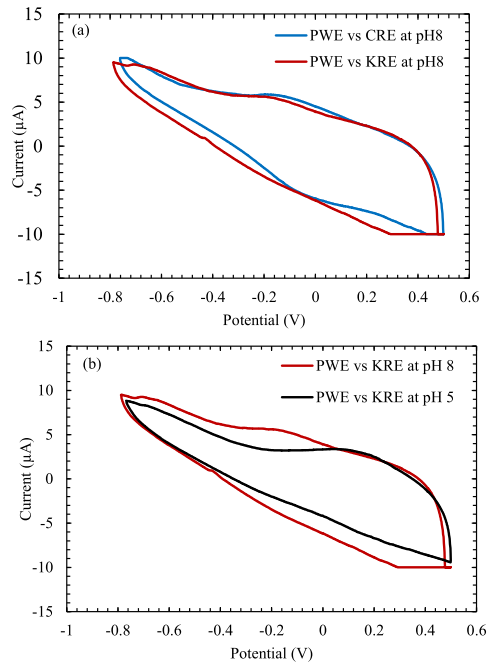


FIGURE 2. Cyclic voltammetry (CV) comparison (a) of PWE vs CRE and PWE vs KRE in the pH 8 solution; and (b) of PWE vs KRE in pH 8 and pH 5 solutions.

of PBS solution. The pH changes were validated by the digital pH meter. Phosphate buffer saline was used for its relevance to body fluid. The PWE with the size of $2 \text{ mm} \times 15 \text{ mm}$ was used as the working electrode and a platinum foil with a diameter of 1.3 cm was used as the counter electrode (CE). For the CV measurements, three electrodes (PWE, CE, KRE or CRE) were immersed in the 50-mL solution and a constant scan rate of 10 mV/s in the potential range from -0.9 V to $+0.5 \text{ V}$ was applied.

Fig. 2 (a) shows similar redox peaks and shapes in the CV curves of PWE against glass-bodied reference electrode (CRE) or flexible Ag/AgCl reference electrode (KRE) in pH 8. This validated that the smaller and deformable KRE can be used with PWE to generate sufficient output potentials. CV measurements performed in the PBS at pH 8 and 5 using PWE and KRE are shown in Fig. 2(b). It shows that the pH 8 case exhibited a broader curve compared to its counterpart at pH 5. The broader curve might be due to higher OH^- groups in the pH 8 buffer solution which produced a higher charging current. A broader CV curve at a higher pH was also observed in [52] which had similar redox peaks for different pH solutions with symmetrical cathodic and anodic shapes.

These experiments verified the feasibility of utilizing the planar flexible PWE and KRE electrodes. The small form-factor of them allows integration in electronic bandages where electrodes have to be conformable, breathable, and small.

B. DEFINITIONS

To ensure the clarity of characterization comparison, the definition terms on performance such as hysteresis, response

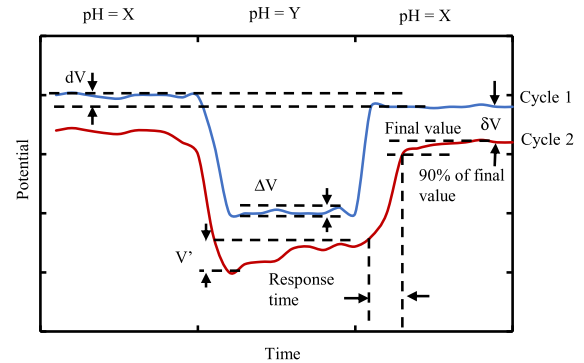


FIGURE 3. Definition of parameters for pH output potential characterization.

time, and stability are summarized in Fig. 3, previously defined by our group. In the time domain, hysteresis (dV) is defined as the standard error of settled potentials at the same pH level tested continuously in one cycle. One cycle here means that the devices are tested in a sequence of pH 2-4-7-10-13-10-7-4-2. Surface modification due to repeated tests in highly acidic and alkaline solutions may establish new equilibrium on the interface between oxide and solution which change electrical impedances and potential outputs. The micro-/nano-scale porous structures on the electrode surface can also be affected by the attachment of molecules from the solution, as well as the aging and oxide formation processes described in [53]. Other factors such as residues, hydration, and oxidation state changes of the porous metal oxide film may also cause hysteresis [21]. It is a common phenomenon observed in metal oxides [54], [55].

Response time is the time taken to reach 90% of the settled potential [25], which includes the time taken for the polymeric membrane to be fully hydrated and reach the redox equilibrium. Sensor stability is evaluated in one test for a certain pH level after the output potential seems settled. In a practical environment, random hydrodynamic motions in a micro-environment caused by air bubbles and external vibrations around the micro/nano-pores in the sensing area can affect electrical potentials and thus sensor stability. Huang et. al [56] categorized stability parameters with potential drift (V') when electrodes stay in the same solution for a period of time; deviation (δV) when electrodes are in the same pH solution in different cycles; and potential fluctuation (ΔV) in which the potential fluctuates but stays stable within a small range of potential; to determine the environmental factors affecting pH performance. The deviation (δV) is defined to be different from the hysteresis (dV) as the deviation may be caused by a capacitive potential shift induced from electrostatic charges accumulated on the surfaces.

C. pH RESPONSE OF PWE IN WIDE pH RANGE OF pH 2 TO 13

The PWE against KRE electrodes were first investigated in standard buffer solutions in a wide pH range from pH 2 to

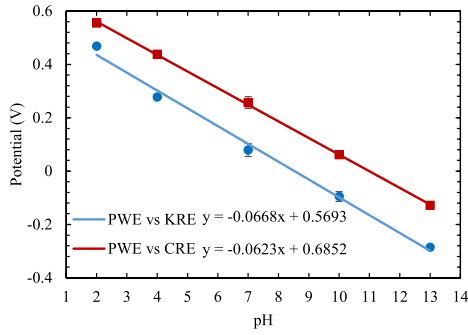


FIGURE 4. Comparison of sensitivities using polyimide-based (blue) and commercial (red) reference electrodes. PWE means PPMM-based working electrode.

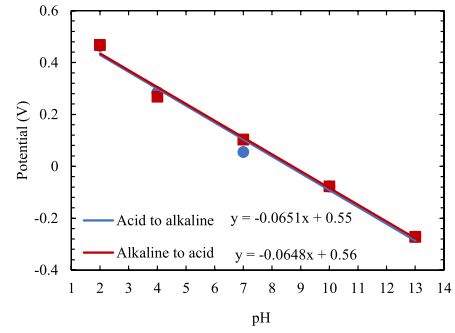
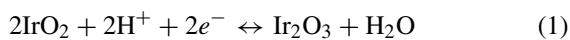


FIGURE 5. Sensitivities of PWE vs KRE tested in buffers solution in sequences from acid to alkaline (2-4-7-10-13), and from alkaline to acid (13-10-7-4-2).

pH 13. The glass-rod reference electrode (CRE) was used for comparison with the flexible Ag/AgCl reference electrode (KRE). The electrodes were cleaned in deionized (DI) water for 30 s between different pH solutions to remove residues, which may produce hysteresis and increase response time.

Fig. 4 shows the PPMM (PWE vs KRE) device sensitivity with 2 mm × 15 mm sizes tested in commercial buffer solutions at pH 2, 4, 7, 10, and 13, also compared to the case of PWE vs CRE. The error bar denotes hysteresis (dV) in respective tests. Both PWE vs CRE and PWE vs KRE show super-Nernstian sensitivities of -62.3 mV/pH and -66.8 mV/pH, respectively. The differences in output potentials by two different types of reference electrodes did not affect the sensitivities significantly. The slight discrepancy in the sensitivities may be due to the ion exchange effects on the surface interfaces of Ag/AgCl or glass membrane. To compare, Chou et al. [46] reported a higher sensitivity of -74.45 mV/pH for a larger PWE size of 1 cm × 1 cm. The larger sensing area likely provides more active sites for ion exchanges, decreases the overall electrical impedance and increases sensitivity.

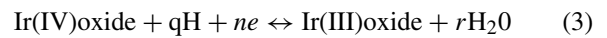
Discrepancies for sensitivity exist over the exact iridium oxide redox mechanisms from the differences in the fabrication processes and a combination of oxy, hydroxy, and ionic species present on the electrode surfaces. The widely accepted redox equilibrium for pH-dependency between two oxidation states is [19], [57].



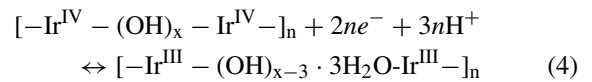
$$E = E_0 - (2.303 \frac{RT}{F})\text{pH} \quad (2)$$

where R is the universal gas constant, T is the temperature and F is the Faraday's constant, and RT/F is equal to 25.688 at 25°C. E_0 is the electrode potential which depends on the type of reference electrode. Ideally, the Nernstian response is -59 mV/pH at room temperature. However, Iridium oxide is known to exist in various oxidation states [58], in addition to redox behaviors, extra protonation in a porous film can produce a higher sensitivity deviating from the Nernstian response [54]. The general reaction for Super-Nernstian

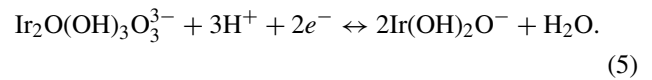
behavior is described as [56], [59], [60], [61].



here values of n, q, and r vary with the oxide preparation method,



and



The redox reaction (4) shows that pH responses are dependent on the oxidation states and can deviate from the value of -59 mV/pH.

Two distinctive test sequences for the sensitivity study in Fig. 5 show sensitivities of -65 mV/pH for the acid to alkaline (2-4-7-10-13) steps, and -64.8 mV/pH for alkaline to acid (13-10-7-4-2) steps. Symmetrical cathodic and anodic peaks in the CV analysis [45] indicated similar potentials generated at particular pH levels, which resulted in similar sensitivities for both sequences. The multiple oxidation states of Ir^{3+} , Ir^{4+} , and Ir^{5+} during CV analysis [45] agreed well with the super-Nernstian response of the PWE electrode. Olthius et al. demonstrated the pH sensitivity as a function of oxidation state [54] and showed a higher oxidation state due to extra protonation could produce a super-Nernstian sensitivity [59].

Fig. 6(a) shows an example of the potential outputs of PWE vs KRE immersed in buffer solutions for 60 secs in five different pH solutions. Electrodes were tested in the sequence pH 2-4-7-10-13-10-7-4-2 as one cycle. Distinct output potentials for different pH levels show stability over 30 s. The electrode pair was then tested in 2 cycles. The potential fluctuation (ΔV) at pH 2, 4, 7, 10 and 13 were 0.3, 0.6, 1.5, 0.6 and 3.7 mV, respectively. The potential deviation (δV) at pH 2, 4, 7, 10, and 13 were 1.7, 5.7, 8.9, 14.7, and 17.6 mV, respectively. Low ΔV and δV mean stable output potentials and accurate pH distinction. The potential drift (V') at pH 2, 4, 7, 10, and 13 were 1.1, 3.7, 8.7, 0.6 and 32.2 mV,

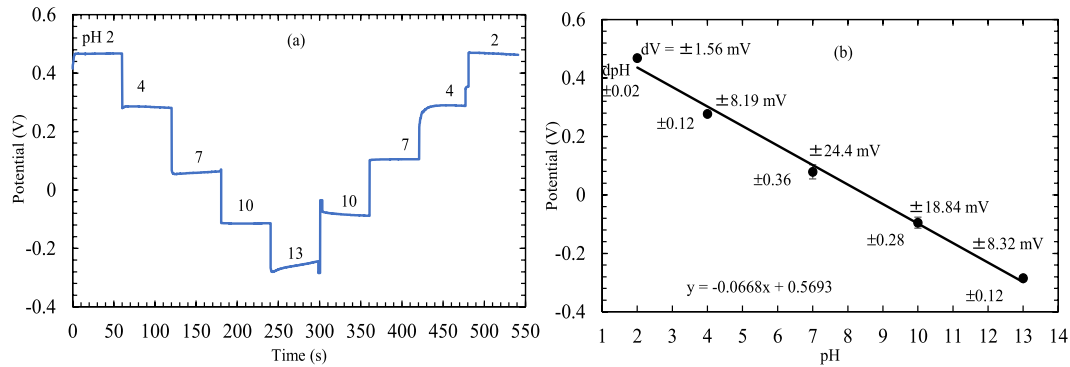


FIGURE 6. (a) Temporal response of PWE vs KRE in one test cycle with buffers at pH 2-4-7-10-13-10-7-4-2. (b) The corresponding pH error (dpH) calculated from the hysteresis (dV) at the respective pH levels.

respectively. Increased drift (V) at pH 13 is probably due to higher and larger OH⁻ groups in the strong alkaline solution than in acidic solution [62], [63].

Fig. 6(b) shows the pH hysteresis (dpH) calculated from potential hysteresis (dV). Hysteresis (dpH) was calculated from dV obtained at the settled potentials according to the sensitivity -66.8 mV/pH. The highest dpH of ± 0.36 at pH 7 was likely due to hysteresis caused by hydroxyl groups trapped in the porous and OH⁻ rich PPMM fibers. The lowest dpH of ± 0.02 at pH 2 was because of faster ionic diffusion of small H⁺ ions between the electrode surface and buffer solution. To validate, the PWE against CRE at pH 7 also produced the highest dV of ± 22.2 mV, compared to other pH levels. After calibration using the sensitivity curve of PWE vs CRE, the pH was also found to be ± 0.36 . This indicates that the higher hysteresis at pH 7 is likely due to the porous nature of the PWE. Because the steps before pH 7 solution were either pH 4 or 10, the residues in the pores became different types - mainly either acidic or mainly alkaline ones. Therefore, the hysteresis effect at pH 7 became inevitably more apparent. Nonetheless, the similar performance of KRE and CRE provides the feasibility of using planar reference electrodes.

The response time of the PPMM sensor was measured by switching from acidic to alkaline (pH 2 to 13) and alkaline to acid (pH 13 to 2) solutions. Fig. 7 shows the response time of 4 s and 6 s when switched from pH 2 to 13 and pH 13 to 2, respectively. Previously, the response time was measured as 3 s and 4 s, tested in the same fashion utilizing the PWE against a commercial glass-rod electrode (CRE) [37].

1) pH RESPONSES IN SMALLER pH RANGES

A smaller pH range from pH 5 to 8 was tested for the PWE vs KRE pair in commercial buffer solutions. A sensitivity of -76.5 mV/pH was obtained for the smaller pH range compared to that of -66.8 mV/pH for the wider range from pH 2 to 13. The electrodes then were tested in the solutions at pH 6.5, 7, and 7.5. These solutions were made from the commercial buffer pH 8 solution by adding 2-M HCl. The pH value was validated by the commercial pH meter.

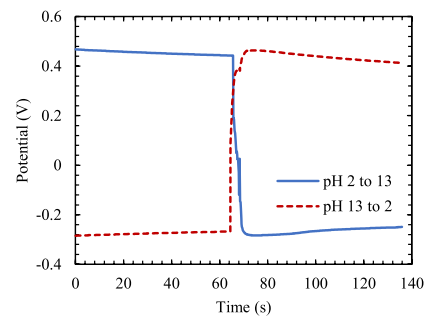


FIGURE 7. Response time of the PWE vs KRE pair between two pH buffer levels.

A sensitivity of -75.7 mV/pH was obtained from the three points of pH 6.5, 7, and 7.5. The test results are plotted in Fig. 8. Lower sensitivity in the wide range from pH 2 to pH 13 may be due to electrodes being tested in highly acidic and alkaline solutions. Although electrodes were cleaned in deionized water, residues in the nano-scale pores were inevitably more and hindered ion exchange. The output potentials tested in smaller ranges fitted well with the overall calibration curve obtained by a wide pH range.

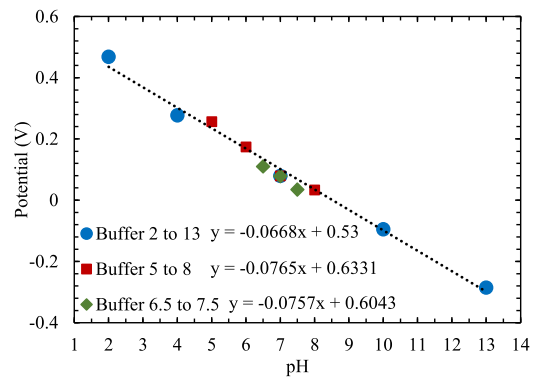


FIGURE 8. Nernstian responses of PWE Vs KRE tested in different pH ranges from buffer 2 to 13 (blue), buffer 5 to 8 (red), and buffer 6.5 to 7.5 (green).

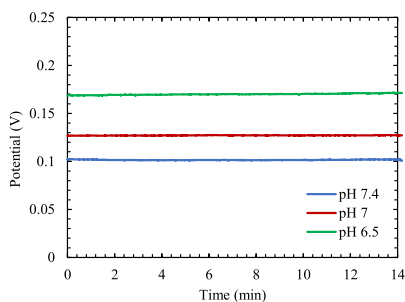


FIGURE 9. Stability in the PBS solutions at pH 7.4, 7, and 6.5.

The electrodes were tested in PBS solution around pH 7 for 14 minutes to investigate their stability in a similar environment to a biological one. The PBS solution with a pH value of 7.4 was adjusted to pH 7 and 6.5 by adding 2-M HCl acid, validated with the commercial pH meter. Fig. 9 shows the stable and distinct output potentials of the PWE vs KRE in three different pH levels. It should be noted that the PBS solution contains 0.137-M NaCl, thus the output potentials were slightly higher than those in the pure buffer solutions.

D. INTERFERENCE EFFECTS

The interference studies using sodium and potassium salts were performed at pH 7.5, 7, and 6.5. Commercial buffer pH 8 was used as the base solution as it being closer to body fluid [64]. pH 7.5, 7, and 6.5 with the addition of 2-M HCl acid were prepared and validated by the commercial pH meter. Lab-grade NaCl and KCl salts were weighed separately and added to 50 ml solutions with different pH values. Figs. 10 (a) and (b) show the signals within 30 s in pH 7.5, 7, and 6.5 solutions that have NaCl and KCl concentrations of 0.1, 0.5, and 1 M. The addition of salt makes the solution seem more acidic with increased output potentials when more salt was added. It was clear that the sensitivity became less in a solution with a higher concentration of salt as the potential steps became smaller. The interference molecules prevent ion exchange on the interface. It should be noted that the sodium and potassium concentrations used (0.5 and 1M) in the experiments were much higher than those in the extracellular fluid (140 mM and 3.5mM for sodium and potassium, respectively) in order to examine their extreme effects [65].

Previously, Yang et al. [51] demonstrated that integrating an array of pH and salt sensors can correct the potential shifts caused by adding salt. The shifted output potential due to additional salt may cause a pH change (ΔpH), which needs to be calibrated. Two types of calibrations were performed at unknown and known salt concentrations. The ΔpH in Figs. 11 (a) and (b) are for NaCl and KCl, respectively. The darker color bars indicate the pH changes when salt concentrations are unknown. The output potentials measured by pH 7.5, 7, and 6.5 calibration solutions (no salt added) were used to obtain the sensitivity slope. Then the sensitivity was used to find the changed pH values after salt addition. The original pH value of 7.5 became pH values of 6.58, 6.04,

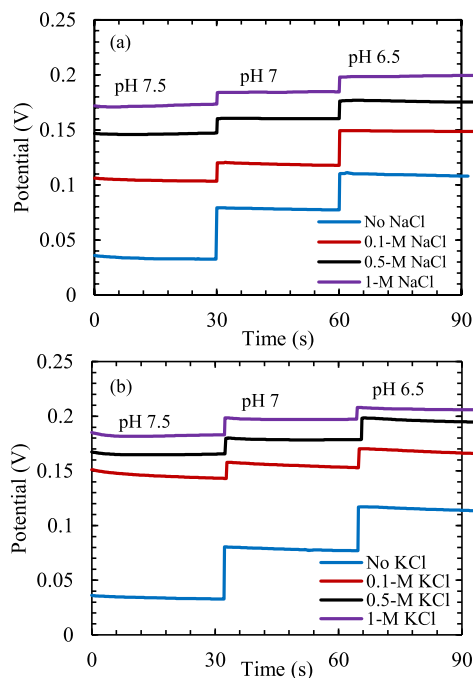


FIGURE 10. Distinct output potential at different pH levels without and with 0.1, 0.5, and 1-M addition of (a) NaCl and (b) KCl salt.

and 5.71, after 0.1 M, 0.5 M, and 1 M NaCl salt was added, respectively, corresponding to ΔpH of 0.9, 1.44, and 1.76. Similarly, using the same sensitivity slope without salt added, the original pH value of 7.5 changed to pH 6.12, 5.91, and 5.7, after 0.1 M, 0.5 M, and 1 M KCl salt was added, respectively, which created ΔpH of 1.37, 1.58, and 1.79 after salt addition. The pH changes (ΔpH) are indicated in the darker color bars also for the cases of pH 7 and pH 6.5 in Fig. 10. When the salt concentrations were measured, the sensitivity slopes at 0.1 M, 0.5 M, and 1 M NaCl or KCl concentrations were employed to find the corresponding ΔpH . The ΔpH at pH 7.5 decreased to 0.07, 0.01, and 0.01, for NaCl; and 0.04, 0.02, and 0.03, for KCl, with 0.1 M, 0.5 M, and 1 M salt addition, respectively. The decreased ΔpH at the known salt concentrations were also observed at pH 7 and 6.5, as shown in the lighter color bars in Figs. 11 (a) and (b).

For comparison, measured pH changes by a commercial pH meter (A211, Orion) when sodium salt concentrations increased from 0 to 1 M for pH 7.5, 7, and 6 were 7.1, 6.61, and 6.08, respectively. For potassium concentrations increased from 0 to 1M, the pH changed to 6.8, 6.3, and 5.86, respectively. It is clear that the PPM sensing fiber-based electrodes have higher interference effects from salt, likely due to the porous nature of the films, compared to conventional glass-based pH electrodes.

E. ELECTRODE TEST PROTOCOLS

The experiments so far were performed with DI water cleaning before every test with the intention to study electrode performance in a situation that has fewer interference factors.

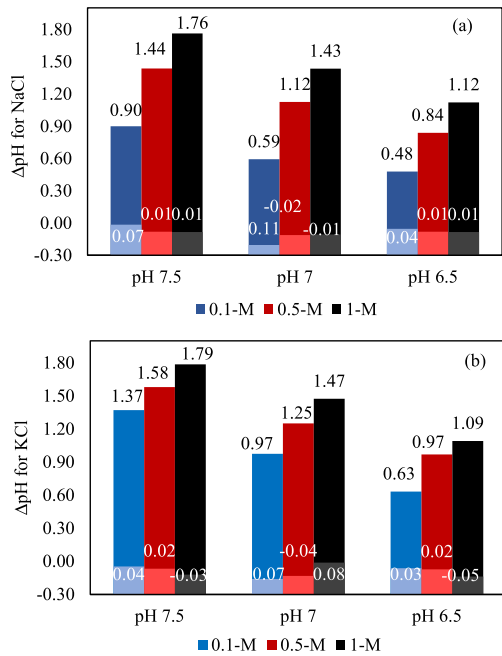


FIGURE 11. The Δ pH after the pH calibration obtained at unknown (darker colors) and known (lighter colors) (a) NaCl and (b) KCl concentrations. The Δ pH is pH difference between the pH value of original buffer solution and that after of the solution with NaCl or KCl added.

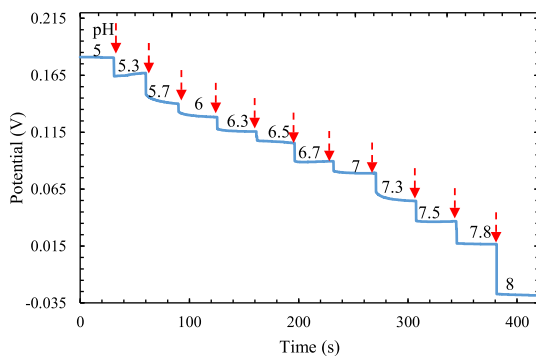


FIGURE 12. PPMM-based pH electrode beaker tested in different pH solutions: 5, 5.3, 5.7, 6, 6.3, 6.5, 6.7, 7, 7.3, 7.5, and 7.8. The red arrow denotes when electrode is switched between beakers. No DI water cleaning to study real scenario.

An experiment without cleaning was performed with finer pH change steps from pH 7.8 to pH 5. Skin wound typically has a pH level around pH 8 [66], [67]. So, the pH 8 buffer was used as the base solution, and only HCl was added, in order to keep the chemical compositions similar in all solutions, to adjust the pH values. The buffers were prepared and mixed well in 50-ml beakers and their pH values were confirmed by a commercial pH meter (A211, Orion). Fig. 12 shows the potential changes when the electrodes were immersed for 30 s sequentially in different pH solutions from acidic to alkaline conditions. The observed longer settling time in pH 7.8 and smaller potential step in pH 6.5 were probably because of accumulated residues on the electrode surfaces.

Fig. 13 shows a titration setup with the PWE vs KRE pair and a commercial pH electrode immersed in the buffer pH 8 solution. The pH level was adjusted by sequentially dripping 20- μ L 2-M HCl acid in the 250-ml buffer to pH 7.5, 7, 6.5, 6, 5.5, and 5. The PWE vs KRE potential was recorded at a sampling rate of 7 S/s while the pH meter showed the discrete pH value after stabilization, which typically took several seconds. The PPMM electrode pair and commercial pH electrode were separated by 6 cm to prevent ion interaction between them. A magnetic stirrer gently mixed the added acid into the solution for 60 s at a low speed of 30 rpm to prevent turbulence. The recording started 30 s after the stirrer stopped. The inset in Fig. 13 (b) shows the distinct PPMM electrode output potentials. The PWE vs KRE output potentials were converted to pH values from the sensitivity slope and compared to the pH values from the pH meter in Fig. 13 (b). The result shows reasonable agreement.

F. VISCOSITY EFFECTS

To investigate the effects of viscosity on electrical output potentials, the planar PWE vs KRE electrodes were tested in a solution with a lower viscosity of 1.2 cP, close to the blood viscosity, and a higher one of 45 cP, similar to the one for serous fluid [68]. The electrodes were also tested at the room temperature (25°C) and body temperature (37°C). Acidic pH 6 buffer was used as the base solution since skin pH starts to become acidic during the wound healing process [69]. Lab-grade starch powders of 1% and 2.4% by weight were added to 50 mL of the pH 6 solution to reach viscosities of 1.2 cP and 45 cP, measured by the capillary tube viscometer (CANNON Instrument). Fig. 14 shows the output potential consistently decreased at 25°C and 37°C as viscosity was increased from 1.2 cP to 45 cP. The reason is likely that the Amylopectin from starch granules aggregates which prevents ionic movement in the viscous matrices and decreases the output potential [70].

With the three-point calibration slope of output potential at known aqueous pH levels 5, 6, and 7, the potentials were converted to find pH values for viscous solutions. The pH changes (Δ pH) between the aqueous and viscous solutions, 1.2 cP or 45 cP, were 1.1 and 0.62 at 25°C, respectively. The Δ pH became 0.89 and 0.54 at 37°C, respectively. The commercial pH meter was also used to measure the aqueous and viscous solutions. Results showed Δ pH as 0.24 and 0.14 at 25°C for viscous 1.2 cP and 45 cP solutions, respectively, compared to the aqueous one. The values became 0.25 and 0.12 at 37°C. Both the planar PWE vs KRE electrode pair and the glass-bodied pH meter confirmed changes in outputs due to viscosity and temperature. The higher Δ pH for the PWE in viscous solution is likely due to large amylopectin starch molecules on the porous membrane, which have more significant effects on the pores between PPMM fibers because of the comparable sizes and prevent ion exchanges on the IrO₂ particles. The temperature dependence is expected as described in Eq. (2).

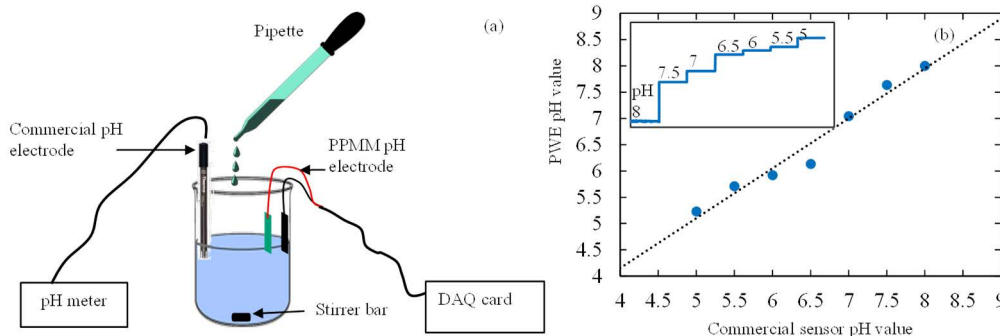


FIGURE 13. (a) Titration setup with a commercial pH meter to validate pH changes, and the PWE vs KRE electrode pair to continuously detect the output potential as HCl is added. (b) The pH values of the PWE vs KRE pair, calculated by the sensitivity curve, are compared to the pH values obtained from the pH meter. The inset shows distinct potentials.

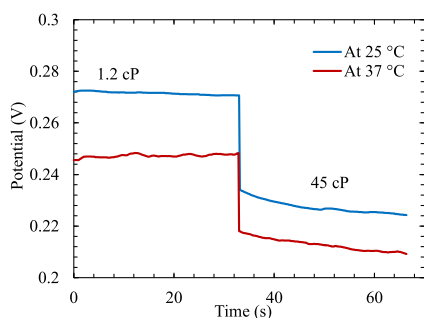


FIGURE 14. The output potential of the PWE vs KRE electrode pair in the pH 6 solution with two different viscosities of 1.2 and 45 cP at 25°C and 37°C.

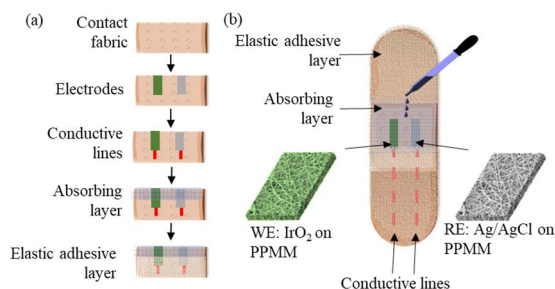


FIGURE 15. (a) Assembling of electrodes in a bandage. (b) pH buffer solution was dripped on the absorbing layer and reached onto the electrodes.

G. BANDAGE CONFIGURATION

A PPMM-based reference electrode (PRE) was prepared by screen printing Ag/AgCl paste on PPMM. To demonstrate the use of PPMM-based sensing films in electronic bandage applications, the PWE vs PRE pair electrodes were assembled. Fig. 15 (a) illustrates the assembling of PPMM electrodes into a bandage configuration. The electrodes were first placed on cotton contact fabric. Ag/AgCl conductive lines were screen printed on the fabric from the surfaces of PWE and KRE film and extended to the edge of the fabric. An absorbing layer, made of porous compressed cotton fibers, was applied onto the electrodes to allow liquid transfusion. The contact fabric then was placed on an elastic adhesive gauze layer [71]. Two wires were threaded through the gauze layer and connected to the Ag/AgCl by silver epoxy. The gauze layer insulated the conductive lines from liquid yet allowed signal transduction from the exposed IrO₂ PWE and Ag/AgCl KRE area. Fig. 15 (b) shows the experimental setup for temporal pH responses as pH solution was dripped from a pipette onto the porous and fibrous surface.

The test was performed in a smaller pH range between 6.5 and 7.5. 2-M HCl was added to pH 8 based solution to produce solutions with a 0.1 pH step change. The calibration was performed between pH 6.5 and 7.5. The pH values were calculated from the output potentials by the sensitivity slope. The pH accuracy was analyzed in the Clarke error grid as

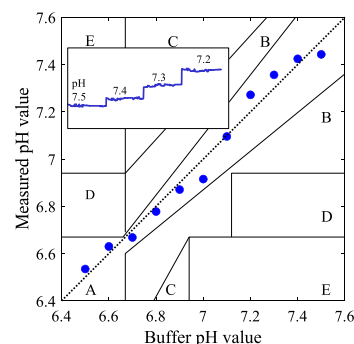


FIGURE 16. Clarke error grid for dripping solutions with 0.1 pH step changes onto the bandage. The inset shows PWE detects pH change in the bandage configuration.

shown in Fig. 16. The inset shows that PWE vs KRE electrode pair in the bandage package can distinguish the 0.1 pH change. The Clarke error grid compares the known buffer pH levels, measured by a commercial pH meter (A211, Orion), and the pH values from the PPMM-based sensor. The data points fell in the zone A indicating acceptable pH accuracy in aqueous pH solutions.

Uric acid plays several important roles in the wound healing processes in the microenvironment of tissue and is considered a major alarmin released by dying cells [72],

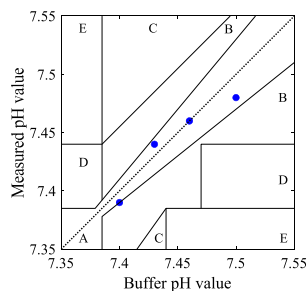


FIGURE 17. Clarke error grid as uric acid (UA) concentration increases in the PBS solution.

[73], [74]. Uric acid was found elevated significantly in wound fluid after tissue injury, with relative concentrations correlated to chronic wound conditions. The severity of a wound can be monitored by sensing the concentration of uric acid or its precursors in wound fluid, as suggested in [75]. Such monitoring is likely to provide information to assess the healing process of the wound. Conventional uric acid detection in blood or urine requires bulky equipment and sufficient samples. The portable testing kit detects uric acid in blood uses disposable test strips and requires a drop of blood obtained by finger prick with a lancet [76], [77]. The method is valuable for monitoring blood in screening gout, cardiovascular diseases, and diabetes [78], [79], however may not be appropriate to monitor wound fluid in situ. Electrochemical enzymatic means enables short-term continuous detection of uric acid and can potentially be a direct assessment of wound [80], [81]. In this work, as the direct detection of uric acid is not our goal, we investigated pH variations due to uric acid concentration changes as one of the precursors in the wound healing process.

Uric acid concentration is reported to be within 220–750 μM in wound fluid [82] Stock solution of 0.1-M uric acid (UA) was prepared by mixing UA powders and 0.1-M phosphate buffer saline solution (PBS) heated at 37°C for solubility. UA concentrations of 200, 400, and 800 μM were prepared from the stock solution and stored in 50-mL beakers. PWE and KRE electrodes were sequentially tested in different UA concentrations without DI water cleaning. The output potential responses were converted to pH values from the calibration curve and compared to the values measured by a commercial pH meter. The results are compared in the Clarke error grid shown in Fig. 17. An increased pH due to UA concentration increases was also observed in [83]. The pH variation due to UA then can be a valuable precursor to determine wound severity.

Since the materials used in the bandage were breathable and conformable, the demonstrated performance gave great promise for monitoring pH variations on skin or wounds.

IV. CONCLUSION

This work demonstrated the fabrication and characterization of an electrical pH sensor based on a porous paper-like material of polypropylene micro membrane (PPMM) for potential applications in skin wound monitoring. Individual PPMM

fibers were conformally coated with gold at 30°C by an electroless process to produce conductive fibers and serve as the base for electrodeposition of IrO_2 nanoparticles. The fabrication technique eliminates the requirement of an elevated temperature in the conventional processes of depositing IrO_2 . The porous, soft, and conformal bioelectrode exhibit mechanical biocompatibility which can be used for paper-based wearables and point-of-care microfluidic devices.

The cyclic voltammetry responses show sufficient charging currents in the small form factor of the planar electrodes. The pH characterization shows Nernstian response in a wide pH range from pH 2 to 13, and smaller ranges between 5 and 8, as well as between 6.5 and 7.5. Parameters related to hysteresis, potential drift, deviation, and fluctuation were investigated. Hysteresis around pH 7 seemed to be more compared to other levels due to the porous nature of the substrates. Other parameters indicated repeatability and stability of the electrodes. Stability was also investigated in phosphate buffer saline (PBS) at pH 6.5, 7, and 7.4, which was similar to the biological environment. Interference effects from salt were investigated with various sodium and potassium concentrations. Calibration at known salt concentrations showed less pH error, indicating the sensing electrodes should be calibrated according to the sodium and potassium concentrations in human body fluids.

Electrode test protocol without water cleansing in the pH range of pH 5 to 8 showed the PPMM-based sensor consistently detected finer pH changes. Comparable pH values to a commercial pH meter during titration showed reliable pH-sensing performance. The pH changes detected by the PPMM-based sensor in viscous solutions at two different temperatures were compared to a commercial sensor. The investigation showed that the planar electrodes should be calibrated for viscous solutions and at the body temperature for their uses in wearables. Electrodes were assembled in a bandage configuration for feasibility studies. The pH values analyzed in a Clarke error grid showed acceptable pH accuracy in the physiological pH range. The increased uric acid concentration causes pH value changes, which could be an important marker for wound conditions.

The chemicals and materials involved in the fabrication of electrodes with negligible bio-toxicity and the biocompatible and gas-permeable properties of polypropylene micro membranes provide advantages of the proposed electronic bandages for wound monitoring. The conductive polymeric membranes, sensing electrodes, and their ability to be integrated with microprocessors and wireless electronics open a new avenue for disposable Internet-of-Things (IoT) wearables and paper-based point-of-care devices. The cost-effective materials and fabrication processes make it beneficial for mass production and large-population applications.

REFERENCES

- [1] L. Manjakkal, D. Szwagierczak, and R. Dahiya, "Metal oxides based electrochemical pH sensors: Current progress and future perspectives," *Prog. Mater. Sci.*, vol. 109, Apr. 2020, Art. no. 100635.

- [2] A. Fog and R. P. Buck, "Electronic semiconducting oxides as pH sensors," *Sens. Actuators*, vol. 5, no. 2, pp. 137–146, Feb. 1984.
- [3] K. Izutsu and H. Yamamoto, "Response of an iridium oxide pH-sensor in nonaqueous solutions. Comparison with other pH-sensors," *Anal. Sci.*, vol. 12, no. 6, pp. 905–909, 1996.
- [4] J. V. Dobson, P. R. Snodin, and H. R. Thirsk, "EMF measurements of cells employing metal—Metal oxide electrodes in aqueous chloride and sulphate electrolytes at temperatures between 25–250°C," *Electrochim. Acta*, vol. 21, pp. 527–533, Jul. 1976.
- [5] M. Ue and J. F. Coetzee, "Potentiometric measurements with an iridium oxide electrode in dimethyl sulfoxide," *Denki Kagaku Oyobi Kogyo Butsuri Kagaku*, vol. 65, no. 5, pp. 401–406, 1997.
- [6] M. Vafaiee, R. Mohammadpour, M. Vossoughi, and P. Sasanpour, "Multi-electrode arrays technology for the non-invasive recording of neural signals: A review article," *Tehran Univ. Med. J. TUMS Publications*, vol. 79, pp. 407–417, no. 6, 2021.
- [7] K. Hungar, M. Görtz, E. Slavcheva, G. Spanier, C. Weidig, and W. Mokwa, "Production processes for a flexible retina implant (Eurosensors XVIII, Session C6.6)," *Sens. Actuators A, Phys.*, vols. 123–124, pp. 172–178, Sep. 2005.
- [8] T. Noda, K. Sasagawa, T. Tokuda, Y. Terasawa, H. Tashiro, H. Kanda, T. Fujikado, and J. Ohta, "Performance improvement and functionalization of an electrode array for retinal prosthesis by iridium oxide coating and introduction of smart-wiring technology using CMOS microchips," *Sens. Actuators A, Phys.*, vol. 211, pp. 27–37, May 2014.
- [9] S. F. Cogan, T. D. Plante, and J. Ehrlich, "Sputtered iridium oxide films (SIROFs) for low-impedance neural stimulation and recording electrodes," in *Proc. 26th Annu. Int. Conf. IEEE Eng. Med. Biol. Soc.*, Sep. 2004, pp. 4153–4156.
- [10] G. Qin, Y. F. Deng, H. M. Zhou, and J. J. Li, "Review of iridium oxide surface modification on bio-electrodes," in *Advanced Materials Research*. Zürich, Switzerland: Trans Tech Publ, 2014, pp. 191–194.
- [11] Y.-M. Chen, T.-W. Chung, P.-W. Wu, and P.-C. Chen, "A cost-effective fabrication of iridium oxide films as biocompatible electrostimulation electrodes for neural interface applications," *J. Alloys Compounds*, vol. 692, pp. 339–345, Jan. 2017.
- [12] C. Chen, S. Ruan, X. Bai, C. Lin, C. Xie, and I.-S. Lee, "Patterned iridium oxide film as neural electrode interface: Biocompatibility and improved neurite outgrowth with electrical stimulation," *Mater. Sci. Eng., C*, vol. 103, Oct. 2019, Art. no. 109865.
- [13] J. D. Weiland, D. J. Anderson, and M. S. Humayun, "In vitro electrical properties for iridium oxide versus titanium nitride stimulating electrodes," *IEEE Trans. Biomed. Eng.*, vol. 49, no. 12, pp. 1574–1579, Dec. 2002.
- [14] R. Fujiwara and I. Shimizu, "Transparent electroconductive film," U.S. Patent 4 670 334 A, Jun. 2, 1987.
- [15] J. E. Baur and T. W. Spaine, "Electrochemical deposition of iridium (IV) oxide from alkaline solutions of iridium (III) oxide," *J. Electroanal. Chem.*, vol. 443, pp. 208–216, Feb. 1998.
- [16] R. K. Jaworski, J. A. Cox, and B. R. Strohmaier, "Characterization of oxide films electrochemically deposited from solutions of palladium chloride and sodium hexachloroaurate," *J. Electroanal. Chem.*, vol. 325, nos. 1–2, pp. 111–123, Mar. 1992.
- [17] M. Wang, S. Yao, and M. Madou, "A long-term stable iridium oxide pH electrode," *Sens. Actuators B, Chem.*, vol. 81, nos. 2–3, pp. 313–315, Jan. 2002.
- [18] R. T. Wimber and H. G. Kraus, "Oxidation of iridium," *Metall. Mater. Trans. B*, vol. 5, pp. 1565–1571, Jul. 1974.
- [19] E. Kinoshita, F. Ingman, G. Edwall, S. Thulin, and S. Głab, "Polycrystalline and monocrystalline antimony, iridium and palladium as electrode material for pH-sensing electrodes," *Talanta*, vol. 33, no. 2, pp. 125–134, Feb. 1986.
- [20] G. Papeschi, S. Bordini, C. Beni, and L. Ventura, "Use of an iridium electrode for direct measurement of pI of proteins after isoelectric focusing in polyacrylamide gel," *Biochim. et Biophys. Acta (BBA)-Protein Struct.*, vol. 453, no. 1, pp. 192–199, Nov. 1976.
- [21] S. Yao, M. Wang, and M. Madou, "A pH electrode based on melt-oxidized iridium oxide," *J. Electrochem. Soc.*, vol. 148, no. 4, p. H29, 2001.
- [22] K. Wang, C. Liu, and D. M. Durand, "Flexible nerve stimulation electrode with iridium oxide sputtered on liquid crystal polymer," *IEEE Trans. Biomed. Eng.*, vol. 56, no. 1, pp. 6–14, Jan. 2009.
- [23] X. Kang, J. Liu, H. Tian, B. Yang, Y. NuLi, and C. Yang, "Sputtered iridium oxide modified flexible parylene microelectrodes array for electrical recording and stimulation of muscles," *Sens. Actuators B, Chem.*, vol. 225, pp. 267–278, Mar. 2016.
- [24] B. Ji, X. Kang, M. Wang, B. Bao, H. Tian, B. Yang, X. Chen, X. Wang, and J. Liu, "Photoelectric neural interface combining wire-bonding μ LEDs with iridium oxide microelectrodes for optogenetics," in *Proc. IEEE 30th Int. Conf. Micro Electro Mech. Syst. (MEMS)*, Jan. 2017, pp. 538–541.
- [25] X. Yang, T. Fu, P. K. Kota, M. Tjia, C. M. Nguyen, and J.-C. Chiao, "Lactate sensors on flexible substrates," *Biosensors*, vol. 6, no. 3, p. 48, 2016.
- [26] C. Nguyen, S. Rao, X. Yang, S. Dubey, J. Mays, H. Cao, and J.-C. Chiao, "Sol-gel deposition of iridium oxide for biomedical micro-devices," *Sensors*, vol. 15, no. 2, pp. 4212–4228, Feb. 2015.
- [27] C. M. Nguyen, W. Huang, S. Rao, H. Cao, U. Tata, M. Chiao, and J. Chiao, "Sol-gel iridium oxide-based pH sensor array on flexible polyimide substrate," *IEEE Sensors J.*, vol. 13, no. 10, pp. 3857–3864, Oct. 2013.
- [28] W.-D. Huang, S. Deb, Y.-S. Seo, S. Rao, M. Chiao, and J. C. Chiao, "A passive radio-frequency pH-sensing tag for wireless food-quality monitoring," *IEEE Sensors J.*, vol. 12, no. 3, pp. 487–495, Mar. 2012.
- [29] X. Li, W. Pei, R. Tang, Q. Gui, K. Guo, Y. Wang, and H. Chen, "Investigation of flexible electrodes modified by TiN, Pt black and IrO_x," *Sci. China Technol. Sci.*, vol. 54, pp. 2305–2309, May 2011.
- [30] A. Osaka, T. Takatsuna, and Y. Miura, "Iridium oxide films via sol-gel processing," *J. Non-Crystalline Solids*, vol. 178, pp. 313–319, Nov. 1994.
- [31] J. Adkins, K. Boehle, and C. Henry, "Electrochemical paper-based microfluidic devices," *Electrophoresis*, vol. 36, pp. 1811–1824, Aug. 2015.
- [32] B. Gao, X. Li, Y. Yang, J. Chu, and B. He, "Emerging paper microfluidic devices," *Analyst*, vol. 144, no. 22, pp. 6497–6511, 2019.
- [33] Z. Nie, C. A. Nijhuis, J. Gong, X. Chen, A. Kumachev, A. W. Martinez, M. Narovlyansky, and G. M. Whitesides, "Electrochemical sensing in paper-based microfluidic devices," *Lab a Chip*, vol. 10, no. 4, pp. 477–483, 2010.
- [34] M. Khalil, S. Wang, J. Yu, R. L. Lee, and N. Liu, "Electrodeposition of iridium oxide nanoparticles for pH sensing electrodes," *J. Electrochem. Soc.*, vol. 163, no. 9, pp. B485–B490, 2016.
- [35] P. Marsh, M. Huerta, T. Le, X. Yang, J.-C. Chiao, and H. Cao, "Wireless iridium oxide-based pH sensing systems," in *Proc. IEEE SENSORS*, New Delhi, India, Oct. 2018.
- [36] S. A. M. Marzouk, S. Ufer, R. P. Buck, T. A. Johnson, L. A. Dunlap, and W. E. Cascio, "Electrodeposited iridium oxide pH electrode for measurement of extracellular myocardial acidosis during acute ischemia," *Anal. Chem.*, vol. 70, no. 23, pp. 5054–5061, Dec. 1998.
- [37] K. Chawang, S.-C. Chou, S. Bing, P.-W. Wu, and J.-C. Chiao, "Characterization of pH sensors based on iridium oxide and gold encapsulated polypropylene membranes," in *Proc. IEEE Sensors*, Oct. 2021.
- [38] S.-G. Jeong, J. Kim, S. H. Jin, K.-S. Park, and C.-S. Lee, "Flow control in paper-based microfluidic device for automatic multistep assays: A focused minireview," *Korean J. Chem. Eng.*, vol. 33, no. 10, pp. 2761–2770, Oct. 2016.
- [39] E. Shirani, A. Razmjou, H. Tavassoli, A. Landarani-Isfahani, S. Rezaei, A. Abbasi Kajani, M. Asadnia, J. Hou, and M. Ebrahimi Warkiani, "Strategically designing a pumpless microfluidic device on an 'inert' polypropylene substrate with potential application in biosensing and diagnostics," *Langmuir*, vol. 33, no. 22, pp. 5565–5576, 2017.
- [40] S.-C. Chou, B.-Y. Sun, T.-L. Fan, Y.-T. Chiang, J.-C. Chiao, and P.-W. Wu, "Fabrication of biocompatible and conductive polypropylene micromembrane as a soft and porous electrode," *J. Taiwan Inst. Chem. Eng.*, vol. 129, pp. 381–388, Dec. 2021.
- [41] G. Sternschuss, D. R. Ostergard, and H. Patel, "Post-implantation alterations of polypropylene in the human," *J. Urol.*, vol. 188, no. 1, pp. 27–32, Jul. 2012.
- [42] N. F. Himma, S. Anisah, N. Prasetya, and I. G. Wenten, "Advances in preparation, modification, and application of polypropylene membrane," *J. Polym. Eng.*, vol. 36, no. 4, pp. 329–362, May 2016.
- [43] T. Le, A. Au-Duong, and C. Lee, "Facile coating on microporous polypropylene membrane for antifouling microfiltration using comb-shaped poly(N-vinylpyrrolidone) with multivalent catechol," *J. Membrane Sci.*, vol. 574, pp. 164–173, Mar. 2019.
- [44] F. C. Usher, J. E. Allen, R. W. Crosthwait, and J. E. Cogan, "Polypropylene monofilament: A new, biologically inert suture for closing contaminated wounds," *Jama*, vol. 179, no. 10, pp. 780–782, 1962.
- [45] S. Chou, B. Sun, W. Cheang, K. Tso, T. Fan, J.-C. Chiao, and P. Wu, "A flexible bioelectrode based on IrO₂-coated metallized polypropylene micromembrane," *Ceram. Int.*, vol. 47, pp. 32554–32561, Dec. 2021.

- [46] S.-C. Chou, Y.-C. Hsieh, W.-H. Cheang, B.-Y. Sun, C.-Y. Chu, S.-Y. Chen, J.-C. Chiao, and P.-W. Wu, "A flexible IrO₂ membrane for pH sensing," *Sci. Rep.*, vol. 12, no. 1, p. 15961, Dec. 2022.
- [47] Y. Zhao, E. A. Hernandez-Pagan, N. M. Vargas-Barbosa, J. L. Dysart, and T. E. Mallouk, "A high yield synthesis of ligand-free iridium oxide nanoparticles with high electrocatalytic activity," *J. Phys. Chem. Lett.*, vol. 2, no. 5, pp. 402–406, Mar. 2011.
- [48] E. M. Jones, C. A. Cochran, and S. L. Percival, "The effect of pH on the extracellular matrix and biofilms," *Adv. Wound Care*, vol. 4, no. 7, pp. 431–439, Jul. 2015.
- [49] W. E. Much and C. S. Wilcox, "Disorders of body fluids, sodium and potassium in chronic renal failure," *Amer. J. Med.*, vol. 72, no. 3, pp. 536–550, Mar. 1982.
- [50] K. Chawang, S. Bing, and J.-C. Chiao, "Investigation of pH Sensing in viscous salt-added solution by iridium oxide film," in *Proc. IEEE Sensors Conf.*, Dallas, TX, USA, Oct./Nov. 2022.
- [51] X. Yang and J.-C. Chiao, "Integrated pH and sodium sensor array based on iridium oxide film," in *Proc. IEEE SENSORS*, New Delhi, India, Oct. 2018.
- [52] K. Wan, Z.-P. Yu, X.-H. Li, M.-Y. Liu, G. Yang, J.-H. Piao, and Z.-X. Liang, "PH effect on electrochemistry of nitrogen-doped carbon catalyst for oxygen reduction reaction," *ACS Catal.*, vol. 5, no. 7, pp. 4325–4332, Jul. 2015.
- [53] B. Aydemir, L. Yagmur, and S. Fank, "Hysteresis errors of commonly used sensor materials," *Measurement*, vol. 43, no. 6, pp. 792–796, 2010.
- [54] W. Olthuis, M. A. M. Robben, P. Bergveld, M. Bos, and W. E. van der Linden, "PH sensor properties of electrochemically grown iridium oxide," *Sens. Actuators B, Chem.*, vol. 2, no. 4, pp. 247–256, Oct. 1990.
- [55] L. Manjakkal, K. Cvejic, J. Kulawik, K. Zaraska, D. Szwagierczak, and G. Stojanovic, "Sensing mechanism of RuO₂-SnO₂ thick film pH sensors studied by potentiometric method and electrochemical impedance spectroscopy," *J. Electroanal. Chem.*, vol. 759, pp. 82–90, Dec. 2015.
- [56] W.-D. Huang, H. Cao, S. Deb, M. Chiao, and J. C. Chiao, "A flexible pH sensor based on the iridium oxide sensing film," *Sens. Actuators A, Phys.*, vol. 169, no. 1, pp. 1–11, Sep. 2011.
- [57] M. L. Hitchman and S. Ramanathan, "A field-induced poisoning technique for promoting convergence of standard electrode potential values of thermally oxidized iridium pH sensors," *Talanta*, vol. 39, no. 2, pp. 137–144, Feb. 1992.
- [58] P. Steegstra and E. Ahlberg, "Influence of oxidation state on the pH dependence of hydrous iridium oxide films," *Electrochim. Acta*, vol. 76, pp. 26–33, Aug. 2012.
- [59] L. D. Burke, J. K. Mulcahy, and D. P. Whelan, "Preparation of an oxidized iridium electrode and the variation of its potential with pH," *J. Electroanal. Chem. Interfacial Electrochem.*, vol. 163, nos. 1–2, pp. 117–128, Mar. 1984.
- [60] T. Katsube, I. Lauks, and J. N. Zemel, "PH-sensitive sputtered iridium oxide films," *Sens. Actuators*, vol. 2, pp. 399–410, Jan. 1981.
- [61] S. Bause, M. Decker, F. Gerlach, J. Näther, F. Köster, P. Neubauer, and W. Vonau, "Development of an iridium-based pH sensor for bioanalytical applications," *J. Solid State Electrochem.*, vol. 22, no. 1, pp. 51–60, Jan. 2018.
- [62] C. N. Tsai, J. C. Chou, T. P. Sun, and S. K. Hsiung, "Study on the time-dependent slow response of the tin oxide pH electrode," *IEEE Sensors J.*, vol. 6, no. 5, pp. 1243–1249, Oct. 2006.
- [63] L. Boussw and P. Bergveld, "The role of buried OH sites in the response mechanism of inorganic-gate pH-sensitive ISFETs," *Sens. Actuators*, vol. 6, pp. 65–78, Sep. 1984.
- [64] W. Aoi, X. Zou, J. B. Xiao, and Y. Marunaka, "Body fluid pH balance in metabolic health and possible benefits of dietary alkaline foods," *eFood*, vol. 1, no. 1, pp. 12–23, Feb. 2020.
- [65] H. R. Pohl, J. S. Wheeler, and H. E. Murray, "Sodium and potassium in health and disease," in *Interrelations between Essential Metal Ions Human Diseases*. New York, NY, USA: Springer, 2013, pp. 29–47.
- [66] L. R. Bennison, C. N. Miller, R. J. Summers, A. Minnis, G. Sussman, and W. McGuiness, "The pH of wounds during healing and infection: A descriptive literature review," *Wound Pract. Res., J. Austral. Wound Manag. Assoc.*, vol. 25, no. 2, pp. 63–69, 2017.
- [67] L. A. Schneider, A. Korber, S. Grabbe, and J. Dissemond, "Influence of pH on wound-healing: A new perspective for wound-therapy?" *Arch. Dermatol. Res.*, vol. 298, no. 9, pp. 413–420, Jan. 2007.
- [68] E. Nader, S. Skinner, M. Romana, R. Fort, N. Lemonne, N. Guillot, A. Gauthier, S. Antoine-Jonville, C. Renoux, M.-D. Hardy-Dessources, E. Stauffer, P. Joly, Y. Bertrand, and P. Connes, "Blood rheology: Key parameters, impact on blood flow, role in sickle cell disease and effects of exercise," *Frontiers Physiol.*, vol. 10, p. 1329, Oct. 2019.
- [69] V. K. Shukla, D. Shukla, S. K. Tiwary, S. Agrawal, and A. Rastogi, "Evaluation of pH measurement as a method of wound assessment," *J. Wound Care*, vol. 16, no. 7, pp. 291–294, Jul. 2007.
- [70] F.-D. Li, L.-T. Li, Z. Li, and E. Tatsumi, "Determination of starch gelatinization temperature by ohmic heating," *J. Food Eng.*, vol. 62, no. 2, pp. 113–120, Apr. 2004.
- [71] X. Liu and P. B. Lillehoj, "Embroidered electrochemical sensors on gauze for rapid quantification of wound biomarkers," *Biosensors Bioelectron.*, vol. 98, pp. 189–194, Dec. 2017.
- [72] R. El Ridi and H. Tallima, "Physiological functions and pathogenic potential of uric acid: A review," *J. Adv. Res.*, vol. 8, no. 5, pp. 487–493, Sep. 2017.
- [73] R. A. Nery, B. S. Kahlow, T. L. Skare, and F. I. Tabushi, "Uric acid and tissue repair," *ABCD. Arquivos Brasileiros de Cirurgia Digestiva (São Paulo)*, vol. 28, pp. 290–292, Nov. 2015.
- [74] J. N. Keller, M. S. Kindy, F. W. Holtzberg, D. K. St. Clair, H.-C. Yen, A. Germeyer, S. M. Steiner, A. J. Bruce-Keller, J. B. Hutchins, and M. P. Mattson, "Mitochondrial manganese superoxide dismutase prevents neural apoptosis and reduces ischemic brain injury: Suppression of peroxynitrite production, lipid peroxidation, and mitochondrial dysfunction," *J. Neurosci.*, vol. 18, no. 2, pp. 687–697, Jan. 1998.
- [75] M. L. Fernandez, Z. Upton, H. Edwards, K. Finlayson, and G. K. Shooter, "Elevated uric acid correlates with wound severity," *Int. Wound J.*, vol. 9, no. 2, pp. 139–149, Apr. 2012.
- [76] K.-S. Dai, D.-Y. Tai, P. Ho, C.-C. Chen, W.-C. Peng, S.-T. Chen, C.-C. Hsu, Y.-P. Liu, H.-C. Hsieh, and S. J. T. Mao, "An evaluation of clinical accuracy of the EasyTouch blood uric acid self-monitoring system," *Clin. Biochem.*, vol. 38, no. 3, pp. 278–281, Mar. 2005.
- [77] A. K. Bhargava, H. Lal, and C. S. Pundir, "Discrete analysis of serum uric acid with immobilized uricase and peroxidase," *J. Biochem. Biophys. Methods*, vol. 39, no. 3, pp. 125–136, May 1999.
- [78] K. L. Rock, H. Kataoka, and J.-J. Lai, "Uric acid as a danger signal in gout and its comorbidities," *Nature Rev. Rheumatol.*, vol. 9, no. 1, pp. 13–23, Jan. 2013.
- [79] Q. Xiong, J. Liu, and Y. Xu, "Effects of uric acid on diabetes mellitus and its chronic complications," *Int. J. Endocrinol.*, vol. 2019, pp. 1–8, Oct. 2019.
- [80] Q. Wang, X. Wen, and J. Kong, "Recent progress on uric acid detection: A review," *Crit. Rev. Anal. Chem.*, vol. 50, no. 4, pp. 359–375, Jul. 2020.
- [81] R. Jirakunakorn, S. Khumngern, J. Choosang, P. Thavarungkul, P. Kanatharana, and A. Numnuam, "Uric acid enzyme biosensor based on a screen-printed electrode coated with Prussian blue and modified with chitosan-graphene composite cryogel," *Microchem. J.*, vol. 154, May 2020, Art. no. 104624.
- [82] N. J. Trengove, S. R. Langton, and M. C. Stacey, "Biochemical analysis of wound fluid from nonhealing and healing chronic leg ulcers," *Wound Repair Regen.*, vol. 4, no. 2, pp. 234–239, Apr. 1996.
- [83] T.-M. Pan and S. Mondal, "Structural properties and sensing characteristics of sensing materials," in *Comprehensive Materials Processing*, vol. 13, S. Hashmi, Ed. Oxford, U.K.: Elsevier, 2014, pp. 179–203.



KHENGDAULIU CHAWANG received the B.Tech. degree in electronics and communication engineering from the National Institute of Technology, India, in 2016, and the M.S. degree in electrical engineering from the University of Texas at Arlington, in 2019. She is currently pursuing the Ph.D. degree in electrical and computer engineering, Southern Methodist University, Dallas, USA.

She has authored/coauthored six peer-reviewed articles on implantable devices and factors affecting pH performance. Her research interests include flexible and ultra-flexible devices by micro and nano fabrication, electrochemical biosensors, wearable electronics, and RF devices.



SHIH-CHENG CHOU received the B.S., M.S., and Ph.D. degrees in the materials science and engineering from the National Yang Ming Chiao Tung University, Hsinchu, Taiwan, in 2015, 2017, and 2021, respectively.

He has authored six peer-reviewed articles on electro-catalysts of fuel cells and polydopamine-related modification techniques. His Ph.D. research explored the fabrication and application of metalized polymeric membrane electrodes and polymeric adhesive layer in the heterogeneous interface of copper and silicon oxide. His research interests include on electrochemical biosensors, pH sensors, and mechanical behavior of flexible electrode.



SEN BING (Graduate Student Member, IEEE) received the B.Tech. degree in electronics and information science and technology from Hainan Normal University, China, in 2013, and the M.S. degree in electrical engineering from Southern Methodist University, in 2019. He is currently pursuing the Ph.D. degree in electrical and computer engineering with Southern Methodist University, Dallas, USA.

He has authored/coauthored one journal article and seven conference papers on optimizing performance for microwave biomedical sensors and implants, four conference papers on factors affecting pH performance, and one conference paper on low-cost ultrasound medical imaging. His research interests include microwave biomedical devices, electro-chemical biosensors, wearable electronics, medical imaging, and RF devices.



PU-WEI WU received the B.S. degree from the Department of Materials Science and Engineering of National Tsing Hua University, Taiwan in 1992, and the Ph.D. degree from the Materials Science and Engineering Department, UCLA, in 1999 under the supervision of Prof. Bruce Dunn.

He was a Technical Manager in New York for five years of industrial experiences. He joined as a Faculty Member at the Department of Materials Science and Engineering, National Yang Ming Chiao Tung University, Taiwan, in 2005. Currently, he is a Full Professor leading a research team of 20 students. He has published around 100 journal articles and has made oral presentations on many international conferences. His research interests include electrophoresis, nanomaterials assembly, and electrochemical sensors.



J.-C. CHIAO (Fellow, IEEE) received the B.S. degree from the Electrical Engineering Department, National Taiwan University in 1988, and the M.S. and Ph.D. degrees in electrical engineering at the California Institute of Technology, in 1991 and 1995, respectively.

He was a Research Scientist at the Optical Networking Systems and Testbeds Group, Bell Communications Research; an Assistant Professor of electrical engineering at the University of Hawaii, Manoa; and a Product Line Manager and a Senior Technology Advisor at Chorum Technologies. He was a Janet and Mike Greene Endowed Professor and a Jenkins Garrett Professor of electrical engineering at the University of Texas–Arlington, from 2002 to 2018. He is currently the Mary and Richard Templeton Centennial Chair Professor of electrical and computer engineering with Southern Methodist University (SMU).

Dr. Chiao was a IEEE MTT Distinguished Microwave Lecturer, from 2012 to 2014, and a IEEE Sensors Council Distinguished Lecturer, from 2017 to 2019. He is a fellow of SPIE, IET, and AIMBE. He was a recipient of the Lockheed Martin Aeronautics Company Excellence in Engineering Teaching Award, the Tech Titans Technology Innovator Award, the Research in Medicine Award in the Heroes of Healthcare, the IEEE Region 5 Outstanding Engineering Educator Award, the IEEE Region 5 Excellent Performance Award, and the 2011 Edith and Peter O'Donnell Award in Engineering by The Academy of Medicine, Engineering and Science of Texas. He was the Chair of the IEEE MTT-S Technical Committee 10 Biological Effect and Medical Applications of RF and Microwave. He is the Chair of 2018 IEEE International Microwave Biomedical Conference (IMBioC) and the Technical Program Chair of 2021 IEEE Wireless Power Transfer Conference. He is an Associate Editor of IEEE TRANSACTIONS ON MICROWAVE THEORY AND TECHNIQUES. He was the founding Editor-in-Chief of the IEEE JOURNAL OF ELECTROMAGNETICS, RF, AND MICROWAVES IN MEDICINE AND BIOLOGY. He is with the Editorial Board of IEEE ACCESS and a Track Editor for IEEE JOURNAL OF MICROWAVES.

...